MATRIX-DRIVEN DETECTION AND RECONSTRUCTION OF LLM WEIGHT HOMOLOGY

Anonymous authors
Paper under double-blind review

ABSTRACT

Recently, concerns about intellectual property in large language models (LLMs) have grown significantly, particularly around the unattributed reuse or replication of model weights. However, existing methods for detecting LLM weight homology fall short in key areas, including recovering the correspondence between weights and computing significance measures such as p-values. We propose Matrix-Driven Instant Review (MDIR), leveraging matrix analysis and Large Deviation Theory. MDIR achieves accurate reconstruction of weight relationships, provides rigorous p-value estimation, and focuses exclusively on homologous weights without requiring full model inference. We demonstrate that MDIR reliably detects homology even after extensive mutations, such as random permutations and continual pretraining with trillions of tokens. Moreover, all detections can be performed on a single consumer PC, making MDIR efficient and accessible.

1 INTRODUCTION

Recent advances in large language models (LLMs) have led to widespread development and adaptation of models trained on massive datasets. While reusing model weights is generally harmless, issues arise when such reusage occurs without proper attribution to the original developers, especially in cases involving direct copying, upcycling (Yao et al., 2024; He et al., 2025), pruning (Ma et al., 2023; Meta-AI, 2024), or continual pretraining. The scale and complexity of LLMs make detection of model weight homology particularly challenging.

Existing methods for detecting model similarity can be broadly classified into two main categories: retrieval-based methods and representation-based methods.

Retrieval-based Methods. Retrieval-based Methods (Xu et al., 2024) rely on vendors embedding specific key-value pairs $\{(k_i, v_i)\}_{i=1,\dots,N}$ into training data, for instance, synthetic hexadecimal strings unlikely to occur naturally. During pretraining, models are optimized to maximize $p_\theta(v_i \mid k_i)$. Downstream models exhibiting anomalously high $p_{\theta'}(v_i \mid k_i)$ (or low perplexity) relative to a random baseline may then be flagged as derived from the original. This approach proved useful in a reported case involving Llama3-V and MiniCPM-o v2.6 (pzc163 et al., 2024), where rare oracle bone inscriptions were used as keys and their corresponding modern Chinese characters as values. However, its effectiveness depends on access to vendor-specific keys or prompts, which pose a significant practical constraint, as such data are rarely disclosed to external users.

Representation-based Methods. Representation-based methods such as REEF (Zhang et al., 2025), HuRef (Zeng et al., 2024), and Intrinsic Fingerprint (He et al., 2025) determine model similarity via comparing internal model representations (either weights directly, or activations under identical inputs). An ideal model similarity measure should be invariant to common transformations (e.g., permutation and scaling) and remain stable even after extensive continual pretraining. While these methods effectively reveal similarity through "fingerprints," they generally lack the ability to reconstruct the weight correspondence mapping (e.g., transformations such as neuron permutation or channel scaling) between models.

Our Method. We propose Matrix-Driven Instant Review (MDIR), a matrix-level similarity detection method. By directly operating on weight matrices, our method identifies not only similarity but also the transformations involved (including permutation and scaling) during model weight reusage.

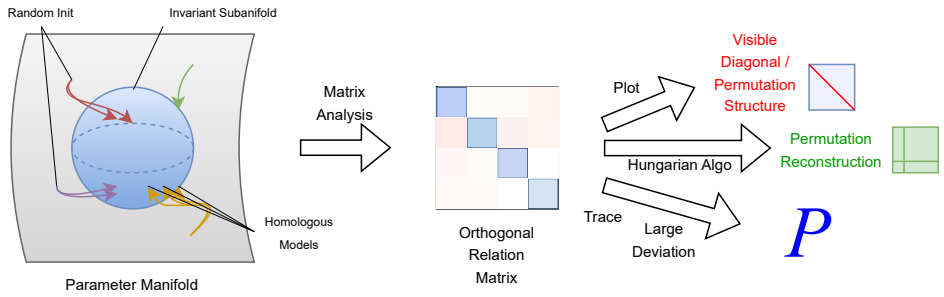

Figure 1: An overall illustration of our MDIR method.

Our method is grounded in a strong mathematical foundation, leveraging Singular Value Decomposition (SVD) and polar decomposition to analyze model matrices. We further utilize Large Deviation Theory (LDT) and random matrix theory to estimate p-values. These mathematical tools provide a rigorous framework for detecting similarities at a fundamental level, making it exceedingly difficult for adversaries to bypass our detection. Moreover, our method also democratizes the verification process. Without requiring access to vendor-specific prompts or specialized hardware, anyone with a standard PC can participate in the verification process. Our main process of MDIR can be summarized in Figure 1.

2 Preliminaries

2.1 Problem Statement

In this paper, we focus solely on weight reuse of large language models and do not address similarities arising from training data selection. Specifically, given two LLMs A and B, with their parameters denoted as θ_A and θ_B, we aim to determine whether A and B exhibit a relationship in their weights, based solely on the statistical properties of θ_A and θ_B. The weight relationships we consider include, but are not limited to, the following cases:

- **Fine-tuning**: Various kinds of SFT and RL included;
- **Continual Pretraining**: Training the model with more data in the general domain, sometimes as much as trillions of tokens;
- **Upcycling** (Yao et al., 2024; He et al., 2025): Continual pretraining with a larger model, especially an MoE model, with weights initialized from a smaller base model (usually dense);
- **Pruning** (Ma et al., 2023; Meta-AI, 2024): Removing certain channels or neurons of a base model to obtain a smaller model;
- **Transformation**: Should include permutations and even general orthogonal/unitary transformations;
- **Comprehensive Combination**: A combination of all these cases above.

This task can be formulated as a binary classification problem Ψ, where the inputs are (θ_A, θ_B) and the output is $\Psi(\theta_A, \theta_B) \in \{0, 1\}$. Here, 1 indicates that the two models are homologous, while 0 indicates unrelated. Due to the vast number of parameters (on the order of billions) as problem input and the scarcity of examples, it is impractical to construct a reliable machine learning framework. Learning-based approach to this task would likely suffer from extreme overfitting without producing trustworthy signals.

2.2 Motivation: Invariant Transformations Preserve Functionality

Modern LLMs are massively overparameterized, meaning many distinct parameter configurations θ and θ' can produce identical input-output behavior: $f_\theta = f_{\theta'}$ even when $\theta \neq \theta'$. These function-

preserving configurations form what we call the **invariant space** of θ:

$$\mathcal{M}_{\text{inv}}(\theta) = \{\theta' \in \mathcal{M}_{\text{arch}} \mid f_{\theta'} = f_\theta\},$$

where $\mathcal{M}_{\text{arch}}$ is the parameter space of the model architecture. However, the structure of the space $\mathcal{M}_{\text{inv}}(\theta)$ is often complicated. It may even vary in dimension (for example, its dimension can be higher when there are n neurons sharing the same input weights in θ).

We seek for a set of transformations, such as orthogonal transformations on the backbone and attention heads, that form a continuous group G that acts on the weights without changing the model's behavior (i.e., the orbit is always generating a submanifold of $\mathcal{M}_{\text{inv}}(\theta)$). We call such transformations **totally invariant**:

Definition 1. *We call a Lie group G acting on $\mathcal{M}_{arch}$ totally invariant if:*

1. *Every $g \in G$ preserves the input-output function: $f_{g\theta} = f_\theta$;*
2. *G acts isometrically (preserves distances in parameter space).*

Note that, we do not need to characterize all totally invariant transformations; We need a subset with sufficiently large dimension, which is enough for subsequent analysis with high confidence. We construct such a group G explicitly for Transformer architectures, especially with GQA, in Section 3.1.

Key Insight: Training Trajectories Preserve G-Coordinates. Under idealized conditions (infinite numerical precision and G-invariant optimizers), training dynamics are confined to the *quotient space* $\mathcal{M}_{\text{arch}}/G$. That is, the component of the parameters along the G-orbit (i.e., within the invariant group) remains unchanged throughout training.

To see why, consider a local orthogonal reparameterization near θ: (α, β), where α parametrizes directions within $G\theta$ (the orbit), and β parametrizes orthogonal directions that actually affect the function. Since the loss is invariant to α, its gradient along α is zero:

$$\frac{\partial \text{Loss}}{\partial \alpha^{(i)}} = 0 \quad \forall i.$$

Thus, under idealized conditions, α remains constant at its initialization value.

If G is an orthogonal subgroup, any orthogonal invariant optimizer is also G-invariant. This accounts for classical SGD and its momentum variants, but not the Adam(W) optimizer. In practice, however, it is unlikely that α deviates significantly from its original coordinates.

Implication for Homology Detection. Suppose two models θ_1, θ_2 are derived from the same initialization (e.g., one is fine-tuned from the other). Then their G-components g_1, g_2 should satisfy $g_1^{-1} g_2 \approx e$, where e is the identity element of the group G. Intuitively, this means that the transformation aligning θ_1 to θ_2 lies close to the identity transformation. In contrast, independently initialized models will have $g_1^{-1} g_2$ distributed randomly across G. This suggests a simple homology detection criterion:

$$\text{If } d_G(g_1^{-1} g_2, e) \text{ is small, then } \theta_1 \text{ and } \theta_2 \text{ are likely homologous,}$$

where $d_G(\_, e)$ can simply be measured by Frobenius inner product, which is equal to the trace ($\langle g, e \rangle_F = \text{Tr}(g)$).

This principle directly enlightens our method MDIR: Using matrix decomposition techniques (SVD / polar), we compute $g_1^{-1} g_2$ and measure its deviation from the identity via the trace. When $g_1^{-1} g_2$ is close to identity, its pattern is clearly visible via the matrix plot. Subsequently, this structural pattern can be converted to statistical significance of p-value via Large Deviation Theory.

3 METHODOLOGIES

3.1 AN INVARIANT TRANSFORMATION GROUP FOR GQA

We assume that model A is the original model and model B the adversary, their parameters denoted as θ_A and θ_B respectively. Both models adopt a decoder-only Transformer architecture (Vaswani

et al., 2017; Radford et al., 2019), with word embeddings and unembeddings, Grouped Query Attention (GQA) (Ainslie et al., 2023), MLP layers with up and down projections (Shazeer, 2020), and RMSNorm layers (Zhang & Sennrich, 2019).

We select GQA for our analysis framework, as GQA represents the most prevalent form of attention mechanism in modern Transformers. Both Multi-Head Attention (with an expansion rate of 1) (Vaswani et al., 2017) and Multi-Query Attention (with one key-value head per layer) (Shazeer, 2019) can be treated as special cases of GQA.

Transformations in the Attention Module. For simplicity, we only consider one layer of attention, namely layer ℓ. Assume that Model B is equivalent to A under certain transformations:

$$\theta_{A,\ell} = \{Q, K, V, O\}$$
$$\theta_{B,\ell} = \{Q', K', V', O'\}.$$

The linear weight transformation from θ_A to θ_B may take the following form:

$$Q' = U_Q Q W_Q, \quad K' = U_K K W_K, \quad V' = U_V V W_V, \quad O' = W_O^{-1} O U_O^{-1},$$

where U_Q, U_K, U_V, U_O and W_Q, W_K, W_V, W_O are transformation matrices applied to the original weights. These matrices represent modifications introduced during model adaptation.

We refer to U_Q, U_K, U_V, U_O as *outer transformations*, which typically correspond to operations such as rotations, permutations, or scaled orthogonal transformations. Since both U_Q, U_K, U_V and Q, K, V operate on normalized vectors:

$$\mathrm{RMSNorm}(x')U_\square = \mathrm{RMSNorm}(x), \quad \square \in \{Q, K, V\},$$

this implies that $U_Q = U_K = U_V$, and they are all orthogonal matrices. In the context of Lie groups, we denote $U_Q = U_K = U_V \in \mathrm{O}(\mathrm{EmbDim})$.

For the *inner transformations* W_Q, W_K, W_V, W_O, the situation becomes more complex due to the presence of attention heads and nonlinear transformations (e.g., Softmax) across channels. Not all orthogonal transformations are permissible for inner transformations.

While we cannot prove that this set encompasses all possible transformations, we provide a sufficient subset:

$$W_Q = \mu \cdot P_1 \otimes P_2 \otimes S, \qquad W_K = \mu^{-1} \cdot P_1 \otimes S,$$
$$W_V = \sum_{v=1}^{\mathrm{NumKVHeads}} (\mathbf{1}_{v,\sigma(v)} \otimes H_v), \quad W_O = \sum_{v=1}^{\mathrm{NumKVHeads}} (\mathbf{1}_{v,\sigma(v)} \otimes P_2 \otimes H_v),$$

where $\otimes$ denotes the Kronecker product of matrices, $\mu \neq 0$ is a scalar, $P_1 \in \mathrm{Perm}(\mathrm{NumKVHeads})$ is a permutation matrix over $\mathrm{NumKVHeads}$ channels (and σ is the corresponding permutation such that $\sum \mathbf{1}_{v,\sigma(v)} = P_1$), $P_2 \in \mathrm{Perm}(\mathrm{QueriesPerHead})$ is a permutation matrix over $\mathrm{QueriesPerHead}$ queries, $S \in \mathrm{diag}(\pm 1, \cdots, \pm 1) \in \mathrm{M}_{\mathrm{HeadDim}}(\mathbb{R})$, and $H \in \mathrm{O}(\mathrm{HeadDim}, \mathbb{R})$ is an arbitrary orthogonal matrix.

To ensure compatibility with both QK-norm (Henry et al., 2020) and RoPE (Su et al., 2023), S is restricted to diagonal matrices with entries ± 1: $S \in \mathrm{diag}(\pm 1, \cdots, \pm 1)$.

We summarize the GQA architecture and invariant transformations in Figure 2, illustrated using Penrose tensor notation, which compactly encodes the tensor contractions and symmetry operations underlying the GQA module.

An Invariant Transformation Group. Comprehensively, the *outer transformations* are directly attached to the model backbone channels (the place where the residual is added), and should be identical across all layers. The *inner transformations*, on the other hand, can be different for each layer. Let $E \in \mathbb{R}^{\mathrm{VocabSize} \times \mathrm{EmbDim}}$ denote the vocabulary embedding matrix (and F the unembedding matrix) of model A, and $E' \in \mathbb{R}^{\mathrm{VocabSize} \times \mathrm{EmbDim}}$ the vocabulary embedding for model B

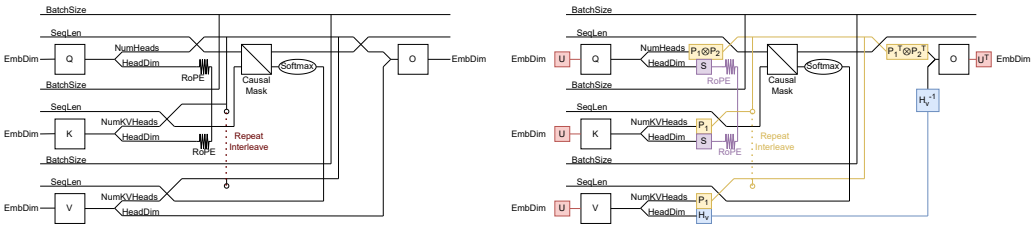

Figure 2: A Penrose notation of a model with Grouped Query Attention architecture (model A, left) and an illustration of an adversary B under application of invariant transformations (right). Bias terms are omitted, and RMSNorms are not explicitly shown.

(and F' the unembedding).

$$
\begin{aligned}
E' &= EU^{\mathrm{T}}, & F' &= UF, \\
Q'_\ell &= UQ_\ell W_{Q,\ell}, & K'_\ell &= UK_\ell W_{K,\ell}, \\
V'_\ell &= UV_\ell W_{V,\ell}, & O'_\ell &= W_{O,\ell}^{-1} O_\ell U^{\mathrm{T}}, \\
W_{Q,\ell} &= \mu_\ell \cdot P_{1,\ell} \otimes P_{2,\ell} \otimes S_\ell, & W_{K,\ell} &= \mu_\ell^{-1} \cdot P_{1,\ell} \otimes S_\ell, \\
W_{V,\ell} &= \sum_{v=1}^{\text{NumKVHeads}} (\mathbf{1}_{v,\sigma_\ell(v)} \otimes H_{\ell,v}), & W_{O,\ell} &= \sum_{v=1}^{\text{NumKVHeads}} (\mathbf{1}_{v,\sigma_\ell(v)} \otimes P_2 \otimes H_{\ell,v}), \\
&(1 \le \ell \le L)
\end{aligned}
$$

The group G can be generated by these elements:

$$U,\ (P_{1,\ell})_{1\le\ell\le L},\ (P_{2,\ell})_{1\le\ell\le L},\ (S_\ell)_{1\le\ell\le L},\ (H_{\ell,v})_{1\le\ell\le L, 1\le v\le \mathrm{HeadDim}}.$$

Whereas U is the component that contributes the most dimension to this group.

3.2 Solving the Transformations

In an idealized setting, we have $E' = EU^{\mathrm{T}}$ for the vocabulary embeddings of models A and B. However, in practical scenarios, the adversary might also have its model trained, perturbing the weight of E'. Following the established conventions, we have:

$$E' = EU^{\mathrm{T}} + N_E,$$

where $U \in \mathbb{R}^{\mathrm{EmbDim}\times\mathrm{EmbDim}}$ is an orthogonal matrix, and N_E represents the additional perturbation introduced by training or noise injection.

To minimize the difference between E' and EX^{T}, we solve the following optimization problem:

$$\min_{X\in\mathrm{O(EmbDim)}} \|E' - EX^{\mathrm{T}}\|_F^2 = \min_{X\in\mathrm{O(EmbDim)}} \left\langle E' - EX^{\mathrm{T}}, E' - EX^{\mathrm{T}} \right\rangle_F.$$

Expanding the Frobenius norm yields:

$$
\begin{aligned}
\arg\min_{X\in\mathrm{O(EmbDim)}} \|E' - EX^{\mathrm{T}}\|_F^2 &= \arg\min_{X\in\mathrm{O(EmbDim)}} \left(\|E'\|_F^2 + \|E\|_F^2 - 2\left\langle EX^{\mathrm{T}}, E' \right\rangle_F\right) \\
&= \arg\max_{X\in\mathrm{O(EmbDim)}} \left\langle EX^{\mathrm{T}}, E' \right\rangle_F \\
&= \arg\max_{X\in\mathrm{O(EmbDim)}} \mathrm{Tr}\left(EX^{\mathrm{T}}E'^{\mathrm{T}}\right) \\
&= \arg\max_{X\in\mathrm{O(EmbDim)}} \mathrm{Tr}\left((E'^{\mathrm{T}}E)X^{\mathrm{T}}\right).
\end{aligned}
$$

We denote $\tilde{U}$ as the solution to this optimization problem. From the trace maximization property, the solution of $\tilde{U}$ is equal to the orthogonal factor in the polar decomposition of $(E'^{\mathrm{T}}E)$. Note that $\tilde{U}$ is not the ground truth of U, but rather a close approximation. To reconstruct the actual U, we seek for

special structural patterns lying behind $\tilde{U}$. For example, if $\tilde{U}$ is sufficiently close to a permutation matrix $P \in \mathrm{Perm}(\mathrm{EmbDim})$, identifiable via:

$$P = \arg\max \mathrm{Tr}(P\tilde{U}^{\mathrm{T}}),$$

then we may safely assert that P is almost equal to the ground truth of U. This problem is equivalent to solving maximum bipartite matching or the linear sum assignment problem (SciPy, 2025), which can be computed in up to $O(n^3)$ time using the Hungarian algorithm. For large matrices (e.g., 18432×18432), solving this exactly may take longer on a CPU.

A unique determination of $\tilde{U}$ requires $(E'^{\mathrm{T}}E)$ to be non-degenerate and full-rank, which necessitates the vocabulary size to satisfy $\mathrm{VocabSize} \geq \mathrm{EmbDim}$. This condition is easily satisfied, as most recent tokenizers have $\mathrm{VocabSize} \geq 3 \times 10^4$.

Changed Tokenizer. When model B uses a different tokenizer, the embedding matrices E and E' are defined over different vocabularies. However, a substantial set of tokens $\mathcal{C}$, including ASCII bytes, common subwords (e.g., `is`, `take`), and morphemes (e.g., `-tion`), is typically shared. In contextualized representations, the meaning (and thus the embedding vector) of a token is determined by its usage across billions of contexts (Mikolov et al., 2013). Consequently, even after independent training, the embeddings of shared tokens in homologous models remain approximately aligned up to the global transformation U. Let $\mathcal{C}$ denote the set of all common tokens. We estimate $\tilde{U}$ as:

$$\tilde{U} = \arg \max_{X \in \mathrm{O}(\mathrm{EmbDim})} \mathrm{Tr}\left(\left(E'[\mathcal{C},:]^{\mathrm{T}}E[\mathcal{C},:]\right)X^{\mathrm{T}}\right).$$

Thus, $\tilde{U}$ corresponds to the orthogonal part in the polar decomposition of $(E'[\mathcal{C},:]^{\mathrm{T}}E[\mathcal{C},:])$.

3.3 Estimating p-value

After identifying a permutation matrix P as $P = \arg\max \mathrm{Tr}(P\tilde{U}^{\mathrm{T}})$. we need a statistical criterion to determine whether our identification is significant. While visual inspection of P and $\tilde{U}$ can provide qualitative evidence, the value of $\mathrm{Tr}(P\tilde{U}^{\mathrm{T}})$ itself serves as a strong quantitative indicator.

Null Hypothesis. Our null hypothesis assumes that models A and B are not homologous, and there is no apparent similarity between their weights. Specifically, we assume that $\tilde{U}$ is uniformly distributed over the orthogonal group $\mathrm{O}(n)$ according to the Haar measure. This assumption is reasonable because under the null hypothesis, there is no systematic relationship between the weights of A and B, and any observed alignment would be purely coincidental.

Below, we take $n = \mathrm{EmbDim}$ for short. Under the assumption of the null hypothesis, the probability measure $\mathrm{d}\mathbb{P}$ should be uniform across all admissible transformations, and the distribution of $\tilde{U}$ should be uniform over $\mathrm{O}(n)$.

Now, fix P_0 as an arbitrary permutation matrix. We estimate the probability of $\mathrm{Tr}(P_0\tilde{U}^{\mathrm{T}}) \geq c$, denoted as:

$$f(c) := \mathbb{P}\left[\mathrm{Tr}(P_0\tilde{U}^{\mathrm{T}}) \geq c\right] = \mathbb{P}\left[\mathrm{Tr}(\tilde{U}) \geq c\right],$$

since $P_0\tilde{U}^{\mathrm{T}}$ and $\tilde{U}$ are both uniformly distributed.

With $n!$ possible permutations, only the one maximizing $\mathrm{Tr}(P\tilde{U}^{\mathrm{T}})$ is chosen. Applying the union bound over all $n!$ permutations yields

$$p \leq n! \cdot \mathbb{P}\left[\mathrm{Tr}(P_0\tilde{U}^{\mathrm{T}}) \geq c\right] = n! \cdot f(c).$$

We estimate the p-value based on the evaluation of $f(c)$. Large Deviation Theory implies $f(c) \leq K\exp(-c^2/2)$ for some constant K. Thus, an upper bound is established as $\log p \leq \log(n!) - c^2/2 + \epsilon$. In practice, we set $\epsilon = 0$ for simplicity. Note that when A and B are homologous, $\mathrm{Tr}(P_0\tilde{U}^{\mathrm{T}})$ scales linearly with n (e.g., $c \approx 0.4n$), so the quadratic term $-c^2/2$ dominates $\log(n!)$, resulting in a highly significant p-value. Please refer to Appendix D for a detailed derivation.

4 EXPERIMENTS

4.1 OVERALL COMPARISON

We select 25 representative models for our comparison to evaluate the effectiveness of our MDIR method. For each pair of models, we compute the trace as $\max \mathrm{Tr}(P\tilde{U}^{\mathrm{T}})$ via $P = \texttt{linear\_sum\_assignment}(\tilde{U})$ (SciPy, 2025). From the right part of Figure 3, we observe that

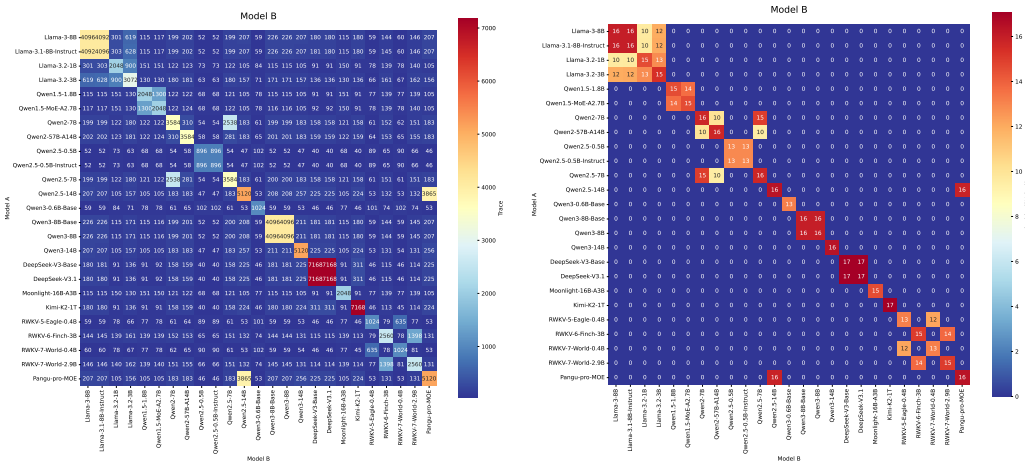

(a) Trace (b) $\log(-\log(p))$

Figure 3: Overall Comparison. We use $\log(-\log(p))$ to crop the p values for better visualization. Value 0 in the right indicates no observable significance.

MDIR for homology detection is self-consistent — it fulfills the requirements of an equivalence relation: reflexivity, symmetry and transitivity. It has also correctly identified all known homology relations, including the following types:

- Instruction fine tuning and continual pretraining: Qwen2.5-0.5B-Instruct (Qwen et al., 2025), Llama-3.1-8B-Instruct (Meta-AI, 2024) and DeepSeek-V3.1 (DeepSeek-AI et al., 2025) are known to have trained from their predecessors;
- Pruning: Llama-3.2-1B and Llama-3.2-3B are pruned from Llama-3.1-8B (Meta-AI, 2024);
- Upcycling: Qwen1.5-MoE-A2.7B (Team) and Qwen2-57B-A14B (Yang et al., 2024) are upcycled from Qwen1.5-1.8B and Qwen2-7B, respectively;
- Non-transformer models: RWKV-7-World-0.4B and 2.9B (Peng et al., 2025) are upgraded from RWKV-5-Eagle-0.4B and RWKV-6-Finch-3B (Peng et al., 2024) respectively;
- Independently developed models: Moonlight-16B-A3B (Liu et al., 2025) and Kimi-K2 (Kimi-Team et al., 2025).

It is worth mentioning that our significance threshold is set purely *a priori*, based on the theoretical p-value bound, without any post-hoc calibration on known positive/negative pairs.

4.2 MATRIX VISUALIZATIONS

We visualize some matrices for several representative cases in Figures 4, 5 and 6.

4.3 ABLATION EXPERIMENT

To demonstrate that MDIR exclusively detects relevance in weights, rather than training data, we conducted an ablation experiment by initializing two models with different random seeds and train-

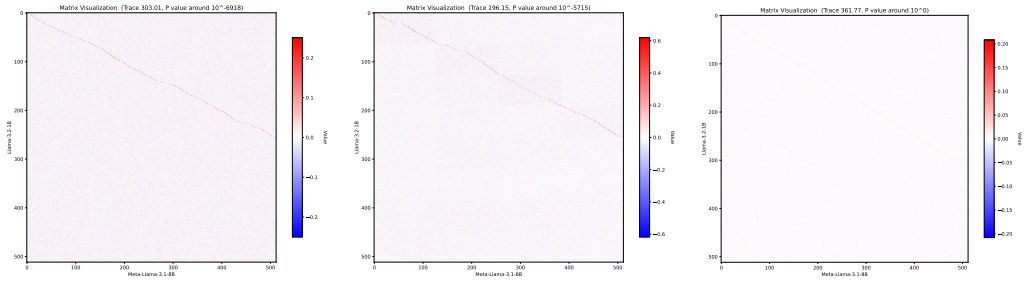

(a) Embedding (b) Layer 3 Attention V (c) Layer 3 MLP Up

Figure 4: MDIR suggests homology between Llama-3.1-8B and Llama-3.2-1B. yielding a p-value of $10^{-6,918}$. For model pruning, the irregular oblique curves (the slope is approximately $1/2$, indicating that half of the channels are retained) can be clearly identified in $\tilde{U}$ from vocabulary as well as inner transformations in the attention module.

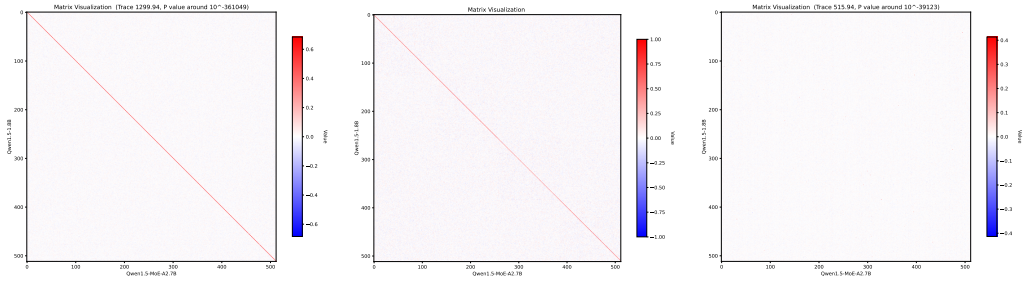

(a) Embedding (b) Layer 9 Attention V (c) Layer 9 MLP Up

Figure 5: For model upcycling, MDIR suggests homology between Qwen1.5-1.8B and Qwen1.5-MoE-A2.7B, yielding a p-value of $10^{-361,049}$. The diagonal patterns for vocabulary embedding and attention modules indicate that these modules are directly inherited from its predecessor, and show no evidence of permutation or channel reselection before the upscaling process.

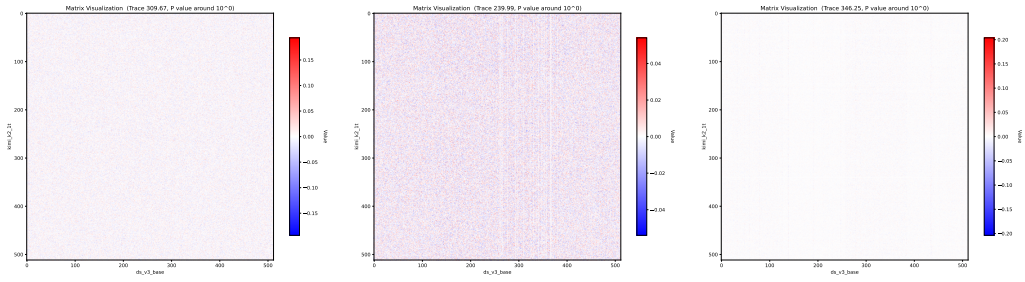

(a) Embedding (b) Layer 0 Attention O (c) Layer 0 MLP Up

Figure 6: For independently developed models, MDIR detects no statistically significant homology between DeepSeek-V3-Base and Kimi-K2-Instruct, with no clear pattern or statistically significant p-value observed.

ing each on two distinct datasets, resulting in a total of 4 models. The datasets were DCLM subsample (Li et al., 2025) (the first 100 files of shard 0 (MLFoundations, 2024), 12.05 billion tokens), and OpenWebMath-ProX (Zhou et al., 2025) (4.61 billion tokens (Gair-ProX, 2024)). Both datasets were tokenized using the GPT-NeoX tokenizer (Black et al., 2022). Models were configured with the `Qwen3ForCausalLM` (HuggingFace, 2025) architecture, with 12 layers and an intermediate size of 1024, resulting in a total of 291 million parameters. They were initialized using HuggingFace `transformers`' default initialization range of 0.02, with random seeds 2 and 3, respectively. All models were trained with a learning rate of linear warmup to 0.002 followed by quadratic decay to 0, and batch size $8(\text{GPUs}) \times 48(\text{sequences}) \times 1024(\text{length})$.

The left two subfigues of Figure 7 reveal clear diagonal patterns for models initialized with the same seed, indicating strong weight similarity due to shared initialization. In contrast, the right two subfigures show no significant outliers and no significance of p-values, even though block-wise patterns are present for inner transformation matrices of attention module. This suggests that models trained on same dataset may develop similar attention features but no substantial weight correlation.

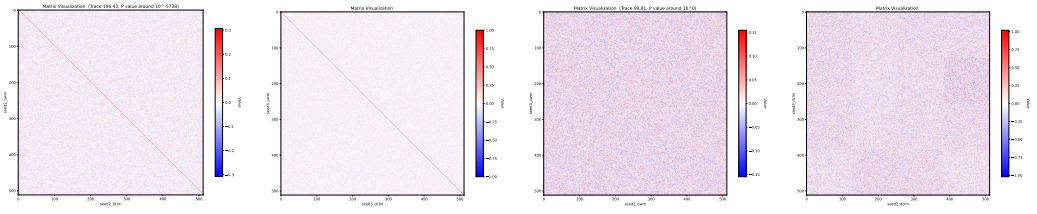

(a) Seed 2, embed (b) Seed 3, Attn V (c) OWM, embed (d) DCLM, Attn V

Figure 7: MDIR only identifies relationship between models initialized with the same seed.

5 Conclusion

We introduced MDIR, a novel method for detecting weight homology in large language models, leveraging matrix analysis and Large Deviation Theory to provide statistically rigorous results. MDIR operates directly on model weights (bypassing full inference) and runs efficiently on a consumer PC, democratizing the verification process. Crucially, MDIR detects weight-level reuse rather than data-level similarity, making it more specific and targeted than previous techniques. This reduces the likelihood of false positives and enhances reliability.

Why Extreme p-values. Our method produces p-values as small as 10^{-10^4} or lower, far beyond typical statistical thresholds. This is not a numerical artifact, but a direct consequence of Large Deviation Theory (LDT). LDT characterizes tail probabilities via rate functions: $p \asymp \exp(-n^2 I(x))$, where n is the model dimension and I is some rate function quantifying deviation from the null. For modern LLMs with $n \gg 1$, this could lead to astronomically small p-values. This reflects the fundamental difference between LLM-scale statistics (billions of parameters) and classical statistical scenarios (hundreds of samples). Such values underflow in floating-point arithmetic but remain well-defined and computable via $\log p$.

Limitation: Numerical Precision. Our analysis assumes infinite numerical precision. In practice, polar decomposition becomes unstable for near-low-rank matrices, and training in low-precision formats (fp16/bf16/fp8) may perturb the Haar-measure assumption. We observed up to 1% discrepancy in the polar factor when switching between fp32 and fp64—though this did not affect detection outcomes in our experiments.

Future Work: Potential Ways of Evading Detection. Although not observed in our experiments, there might be methods to evade our detection. Could MDIR be evaded via more complex adversaries, like additional training with larger learning rates, especially for vocabulary embeddings and attention modules? We leave this for future work.

REFERENCES

Joshua Ainslie, James Lee-Thorp, Michiel de Jong, Yury Zemlyanskiy, Federico Lebrón, and Sumit Sanghai. Gqa: Training generalized multi-query transformer models from multi-head checkpoints, 2023. URL https://arxiv.org/abs/2305.13245.

Noah Amsel, David Persson, Christopher Musco, and Robert M. Gower. The polar express: Optimal matrix sign methods and their application to the muon algorithm, 2025. URL https://arxiv.org/abs/2505.16932.

G.W. Anderson, A. Guionnet, and O. Zeitouni. *An Introduction to Random Matrices*. Cambridge Studies in Advanced Mathematics. Cambridge University Press, 2010. ISBN 9780521194525. URL https://www.wisdom.weizmann.ac.il/~zeitouni/cupbook.pdf.

Ascend Team. Pangu pro moe: A scalable mixture-of-experts model with dynamic grouped routing for efficient large-scale training. *arXiv preprint*, 5 2025. URL https://arxiv.org/abs/2505.21411. Technical report detailing the MoGE architecture and optimization for Ascend NPUs.

Ascend Tribe. Pangu pro moe: A 72b parameter sparse mixture-of-experts model, 6 2025. URL https://ai.gitcode.com/ascend-tribe/pangu-pro-moe-model. Model weights and inference code for Pangu Pro MoE, optimized for Ascend NPUs.

Sidney Black, Stella Biderman, Eric Hallahan, Quentin Anthony, Leo Gao, Laurence Golding, Horace He, Connor Leahy, Kyle McDonell, Jason Phang, Michael Pieler, Usvsn Sai Prashanth, Shivanshu Purohit, Laria Reynolds, Jonathan Tow, Ben Wang, and Samuel Weinbach. GPT-NeoX-20B: An open-source autoregressive language model. In Angela Fan, Suzana Ilic, Thomas Wolf, and Matthias Gallé (eds.), *Proceedings of BigScience Episode #5 – Workshop on Challenges & Perspectives in Creating Large Language Models*, pp. 95–136, virtual+Dublin, May 2022. Association for Computational Linguistics. doi: 10.18653/v1/2022.bigscience-1.9. URL https://aclanthology.org/2022.bigscience-1.9/.

DeepSeek-AI, Aixin Liu, Bei Feng, Bing Xue, Bingxuan Wang, Bochao Wu, Chengda Lu, Chenggang Zhao, Chengqi Deng, Chenyu Zhang, Chong Ruan, Damai Dai, Daya Guo, Dejian Yang, Deli Chen, Dongjie Ji, Erhang Li, Fangyun Lin, Fucong Dai, Fuli Luo, Guangbo Hao, Guanting Chen, Guowei Li, H. Zhang, Han Bao, Hanwei Xu, Haocheng Wang, Haowei Zhang, Honghui Ding, Huajian Xin, Huazuo Gao, Hui Li, Hui Qu, J. L. Cai, Jian Liang, Jianzhong Guo, Jiaqi Ni, Jiashi Li, Jiawei Wang, Jin Chen, Jingchang Chen, Jingyang Yuan, Junjie Qiu, Junlong Li, Junxiao Song, Kai Dong, Kai Hu, Kaige Gao, Kang Guan, Kexin Huang, Kuai Yu, Lean Wang, Lecong Zhang, Lei Xu, Leyi Xia, Liang Zhao, Litong Wang, Liyue Zhang, Meng Li, Miaojun Wang, Mingchuan Zhang, Minghua Zhang, Minghui Tang, Mingming Li, Ning Tian, Panpan Huang, Peiyi Wang, Peng Zhang, Qiancheng Wang, Qihao Zhu, Qinyu Chen, Qiushi Du, R. J. Chen, R. L. Jin, Ruiqi Ge, Ruisong Zhang, Ruizhe Pan, Runji Wang, Runxin Xu, Ruoyu Zhang, Ruyi Chen, S. S. Li, Shanghao Lu, Shangyan Zhou, Shanhuang Chen, Shaoqing Wu, Shengfeng Ye, Shengfeng Ye, Shirong Ma, Shiyu Wang, Shuang Zhou, Shuiping Yu, Shunfeng Zhou, Shuting Pan, T. Wang, Tao Yun, Tian Pei, Tianyu Sun, W. L. Xiao, Wangding Zeng, Wanjia Zhao, Wei An, Wen Liu, Wenfeng Liang, Wenjun Gao, Wenqin Yu, Wentao Zhang, X. Q. Li, Xiangyue Jin, Xianzu Wang, Xiao Bi, Xiaodong Liu, Xiaohan Wang, Xiaojin Shen, Xiaokang Chen, Xiaokang Zhang, Xiaosha Chen, Xiaotao Nie, Xiaowen Sun, Xiaoxiang Wang, Xin Cheng, Xin Liu, Xin Xie, Xingchao Liu, Xingkai Yu, Xinnan Song, Xinxia Shan, Xinyi Zhou, Xinyu Yang, Xinyuan Li, Xuecheng Su, Xuheng Lin, Y. K. Li, Y. Q. Wang, Y. X. Wei, Y. X. Zhu, Yang Zhang, Yanhong Xu, Yanhong Xu, Yanping Huang, Yao Li, Yao Zhao, Yaofeng Sun, Yaohui Li, Yaohui Wang, Yi Yu, Yi Zheng, Yichao Zhang, Yifan Shi, Yiliang Xiong, Ying He, Ying Tang, Yishi Piao, Yisong Wang, Yixuan Tan, Yiyang Ma, Yiyuan Liu, Yongqiang Guo, Yu Wu, Yuan Ou, Yuchen Zhu, Yuduan Wang, Yue Gong, Yuheng Zou, Yujia He, Yukun Zha, Yunfan Xiong, Yunxian Ma, Yuting Yan, Yuxiang Luo, Yuxiang You, Yuxuan Liu, Yuyang Zhou, Z. F. Wu, Z. Z. Ren, Zehui Ren, Zhangli Sha, Zhe Fu, Zhean Xu, Zhen Huang, Zhen Zhang, Zhenda Xie, Zhengyan Zhang, Zhewen Hao, Zhibin Gou, Zhicheng Ma, Zhigang Yan, Zhihong Shao, Zhipeng Xu, Zhiyu Wu, Zhongyu Zhang, Zhuoshu Li, Zihui Gu, Zijia Zhu, Zijun Liu, Zilin Li, Ziwei Xie, Ziyang Song, Ziyi Gao, and Zizheng Pan. Deepseek-v3 technical report, 2025. URL https://arxiv.org/abs/2412.19437.

Amir Dembo and Ofer Zeitouni. *Large Deviations: Techniques and Applications*. Springer, 2 edition, 1998.

P. Diaconis and M. Shahshahani. On the eigenvalues of random matrices. *J. Appl. Probab.*, 31A: 49–62, 1994.

Freeman J. Dyson. Statistical theory of the energy levels of complex systems. *Journal of Mathematical Physics*, 3:140, 1962. doi: 10.1063/1.1703773.

Peter Eichelsbacher, Jens Sommerauer, and Michael Stolz. Large deviations for disordered bosons and multiple orthogonal polynomial ensembles. *Journal of Mathematical Physics*, 52(7), 7 2011. ISSN 1089-7658. doi: 10.1063/1.3603994. URL http://dx.doi.org/10.1063/1.3603994.

Gair-ProX. open-web-math-pro, 2024. URL https://huggingface.co/datasets/gair-prox/open-web-math-pro. The dataset used in this work.

Fabrice Gamboa, Jan Nagel, and Alain Rouault. Sum rules and large deviations for spectral measures on the unit circle, 2017. URL https://arxiv.org/abs/1604.06934.

V. L. Girko. Distribution of eigenvalues and eigenvectors of orthogonal random matrices. *Ukrainian Mathematical Journal*, 37(5):457, 1985. doi: 10.1007/bf01061167.

David J. Gross and Edward Witten. Possible third-order phase transition in the large-n lattice gauge theory. *Physical Review D*, 21:446–453, 1980. doi: 10.1103/PhysRevD.21.446.

Ethan He, Abhinav Khattar, Ryan Prenger, Vijay Korthikanti, Zijie Yan, Tong Liu, Shiqing Fan, Ashwath Aithal, Mohammad Shoeybi, and Bryan Catanzaro. Upcycling large language models into mixture of experts, 2025. URL https://arxiv.org/abs/2410.07524.

Alex Henry, Prudhvi Raj Dachapally, Shubham Pawar, and Yuxuan Chen. Query-key normalization for transformers, 2020. URL https://arxiv.org/abs/2010.04245.

Roger A Horn and Charles R Johnson. *Matrix analysis*. Cambridge university press, 2012.

HuggingFace. Qwen3 model implementation (modeling_qwen3.py), 7 2025. URL https://github.com/huggingface/transformers/blob/main/src/transformers/models/qwen3/modeling_qwen3.py. Source file: modeling_qwen3.py from the Hugging Face Transformers library.

Kurt Johansson. On random matrices from the compact classical groups. *Ann. of Math. (2)*, 145(3): 519–545, 1997.

Kimi-Team, Yifan Bai, Yiping Bao, Guanduo Chen, Jiahao Chen, Ningxin Chen, Ruijue Chen, Yanru Chen, Yuankun Chen, Yutian Chen, Zhuofu Chen, Jialei Cui, Hao Ding, Mengnan Dong, Angang Du, Chenzhuang Du, Dikang Du, Yulun Du, Yu Fan, Yichen Feng, Kelin Fu, Bofei Gao, Hongcheng Gao, Peizhong Gao, Tong Gao, Xinran Gu, Longyu Guan, Haiqing Guo, Jianhang Guo, Hao Hu, Xiaoru Hao, Tianhong He, Weiran He, Wenyang He, Chao Hong, Yangyang Hu, Zhenxing Hu, Weixiao Huang, Zhiqi Huang, Zihao Huang, Tao Jiang, Zhejun Jiang, Xinyi Jin, Yongsheng Kang, Guokun Lai, Cheng Li, Fang Li, Haoyang Li, Ming Li, Wentao Li, Yanhao Li, Yiwei Li, Zhaowei Li, Zheming Li, Hongzhan Lin, Xiaohan Lin, Zongyu Lin, Chengyin Liu, Chenyu Liu, Hongzhang Liu, Jingyuan Liu, Junqi Liu, Liang Liu, Shaowei Liu, T. Y. Liu, Tianwei Liu, Weizhou Liu, Yangyang Liu, Yibo Liu, Yiping Liu, Yue Liu, Zhengying Liu, Enzhe Lu, Lijun Lu, Shengling Ma, Xinyu Ma, Yingwei Ma, Shaoguang Mao, Jie Mei, Xin Men, Yibo Miao, Siyuan Pan, Yebo Peng, Ruoyu Qin, Bowen Qu, Zeyu Shang, Lidong Shi, Shengyuan Shi, Feifan Song, Jianlin Su, Zhengyuan Su, Xinjie Sun, Flood Sung, Heyi Tang, Jiawen Tao, Qifeng Teng, Chensi Wang, Dinglu Wang, Feng Wang, Haiming Wang, Jianzhou Wang, Jiaxing Wang, Jinhong Wang, Shengjie Wang, Shuyi Wang, Yao Wang, Yejie Wang, Yiqin Wang, Yuxin Wang, Yuzhi Wang, Zhaoji Wang, Zhengtao Wang, Zhexu Wang, Chu Wei, Qianqian Wei, Wenhao Wu, Xingzhe Wu, Yuxin Wu, Chenjun Xiao, Xiaotong Xie, Weimin Xiong, Boyu Xu, Jing Xu, Jinjing Xu, L. H. Xu, Lin Xu, Suting Xu, Weixin Xu, Xinran Xu, Yangchuan Xu, Ziyao Xu, Junjie Yan, Yuzi Yan, Xiaofei Yang, Ying Yang, Zhen Yang, Zhilin Yang, Zonghan Yang, Haotian Yao, Xingcheng Yao, Wenjie Ye, Zhuorui Ye, Bohong Yin, Longhui Yu, Enming Yuan, Hongbang

Yuan, Mengjie Yuan, Haobing Zhan, Dehao Zhang, Hao Zhang, Wanlu Zhang, Xiaobin Zhang, Yangkun Zhang, Yizhi Zhang, Yongting Zhang, Yu Zhang, Yutao Zhang, Yutong Zhang, Zheng Zhang, Haotian Zhao, Yikai Zhao, Huabin Zheng, Shaojie Zheng, Jianren Zhou, Xinyu Zhou, Zaida Zhou, Zhen Zhu, Weiyu Zhuang, and Xinxing Zu. Kimi k2: Open agentic intelligence, 2025. URL https://arxiv.org/abs/2507.20534.

Jeffrey Li, Alex Fang, Georgios Smyrnis, Maor Ivgi, Matt Jordan, Samir Gadre, Hritik Bansal, Etash Guha, Sedrick Keh, Kushal Arora, Saurabh Garg, Rui Xin, Niklas Muennighoff, Reinhard Heckel, Jean Mercat, Mayee Chen, Suchin Gururangan, Mitchell Wortsman, Alon Albalak, Yonatan Bitton, Marianna Nezhurina, Amro Abbas, Cheng-Yu Hsieh, Dhruba Ghosh, Josh Gardner, Maciej Kilian, Hanlin Zhang, Rulin Shao, Sarah Pratt, Sunny Sanyal, Gabriel Ilharco, Giannis Daras, Kalyani Marathe, Aaron Gokaslan, Jieyu Zhang, Khyathi Chandu, Thao Nguyen, Igor Vasiljevic, Sham Kakade, Shuran Song, Sujay Sanghavi, Fartash Faghri, Sewoong Oh, Luke Zettlemoyer, Kyle Lo, Alaaeldin El-Nouby, Hadi Pouransari, Alexander Toshev, Stephanie Wang, Dirk Groeneveld, Luca Soldaini, Pang Wei Koh, Jenia Jitsev, Thomas Kollar, Alexandros G. Dimakis, Yair Carmon, Achal Dave, Ludwig Schmidt, and Vaishaal Shankar. Datacomp-lm: In search of the next generation of training sets for language models, 2025. URL https://arxiv.org/abs/2406.11794.

Jingyuan Liu, Jianlin Su, Xingcheng Yao, Zhejun Jiang, Guokun Lai, Yulun Du, Yidao Qin, Weixin Xu, Enzhe Lu, Junjie Yan, Yanru Chen, Huabin Zheng, Yibo Liu, Shaowei Liu, Bohong Yin, Weiran He, Han Zhu, Yuzhi Wang, Jianzhou Wang, Mengnan Dong, Zheng Zhang, Yongsheng Kang, Hao Zhang, Xinran Xu, Yutao Zhang, Yuxin Wu, Xinyu Zhou, and Zhilin Yang. Muon is scalable for llm training, 2025. URL https://arxiv.org/abs/2502.16982.

Xinyin Ma, Gongfan Fang, and Xinchao Wang. LLM-pruner: On the structural pruning of large language models. In *Thirty-seventh Conference on Neural Information Processing Systems*, 2023. URL https://openreview.net/forum?id=J8Ajf9WfXP.

J. C. Mason and D. C. Handscomb. *Chebyshev Polynomials*. Chapman and Hall/CRC, 1st edition, 2002. doi: 10.1201/9781420036114. URL https://mezbanhabibi.ir/wp-content/uploads/2020/01/CHEBYSHEV-POLYNOMIALS-J1.C.-MASOND.C.-HANDSCOMB.pdf.

Madan Lal Mehta. *Random Matrices*. Elsevier Academic Press, Amsterdam, 3rd edition, 2004. ISBN 978-0-12-088409-4.

Meta-AI. Llama 3.2: Revolutionizing edge ai and vision with open, customizable models, September 2024. URL https://ai.meta.com/blog/llama-3-2-connect-2024-vision-edge-mobile-devices/. Blog post announced at Connect 2024 conference.

Meta-AI. Introducing llama 3.1: Our most capable models to date, 7 2024. URL https://ai.meta.com/blog/meta-llama-3-1/. Meta AI Blog.

Tomas Mikolov, Ilya Sutskever, Kai Chen, Greg S Corrado, and Jeff Dean. Distributed representations of words and phrases and their compositionality. In C.J. Burges, L. Bottou, M. Welling, Z. Ghahramani, and K.Q. Weinberger (eds.), *Advances in Neural Information Processing Systems*, volume 26. Curran Associates, Inc., 2013. URL https://proceedings.neurips.cc/paper_files/paper/2013/file/9aa42b31882ec039965f3c4923ce901b-Paper.pdf.

MLFoundations. Dclm-baseline-1.0/global-shard_01_of_10/local-shard_0_of_10, 2024. URL https://huggingface.co/datasets/mlfoundations/dclm-baseline-1.0/tree/main/global-shard_01_of_10/local-shard_0_of_10. Subset of the dataset used in this work.

Bo Peng, Daniel Goldstein, Quentin Gregory Anthony, Alon Albalak, Eric Alcaide, Stella Biderman, Eugene Cheah, Teddy Ferdinan, Kranthi Kiran GV, Haowen Hou, Satyapriya Krishna, Ronald McClelland Jr., Niklas Muennighoff, Fares Obeid, Atsushi Saito, Guangyu Song, Haoqin Tu, Ruichong Zhang, Bingchen Zhao, Qihang Zhao, Jian Zhu, and Rui-Jie Zhu. Eagle and finch: RWKV with matrix-valued states and dynamic recurrence. In *First Conference on Language Modeling*, 2024. URL https://openreview.net/forum?id=soz1SEiPeq.

Bo Peng, Ruichong Zhang, Daniel Goldstein, Eric Alcaide, Xingjian Du, Haowen Hou, Jiaju Lin, Jiaxing Liu, Janna Lu, William Merrill, Guangyu Song, Kaifeng Tan, Saiteja Utpala, Nathan Wilce, Johan S. Wind, Tianyi Wu, Daniel Wuttke, and Christian Zhou-Zheng. Rwkv-7 "goose" with expressive dynamic state evolution, 2025. URL https://arxiv.org/abs/2503.14456.

pzc163 et al. Project author team stay tuned: I found out that the llama3-v project is stealing a lot of academic work from minicpm-llama3-v 2.5, June 2024. URL https://github.com/OpenBMB/MiniCPM-o/issues/196. GitHub issue opened in the MiniCPM-o repository.

Qwen, :, An Yang, Baosong Yang, Beichen Zhang, Binyuan Hui, Bo Zheng, Bowen Yu, Chengyuan Li, Dayiheng Liu, Fei Huang, Haoran Wei, Huan Lin, Jian Yang, Jianhong Tu, Jianwei Zhang, Jianxin Yang, Jiaxi Yang, Jingren Zhou, Junyang Lin, Kai Dang, Keming Lu, Keqin Bao, Kexin Yang, Le Yu, Mei Li, Mingfeng Xue, Pei Zhang, Qin Zhu, Rui Men, Runji Lin, Tianhao Li, Tianyi Tang, Tingyu Xia, Xingzhang Ren, Xuancheng Ren, Yang Fan, Yang Su, Yichang Zhang, Yu Wan, Yuqiong Liu, Zeyu Cui, Zhenru Zhang, and Zihan Qiu. Qwen2.5 technical report, 2025. URL https://arxiv.org/abs/2412.15115.

Alec Radford, Jeff Wu, Rewon Child, David Luan, Dario Amodei, and Ilya Sutskever. Language models are unsupervised multitask learners. 2019. OpenAI blog / technical report.

Robert Schatten. *A Theory of Cross-Spaces. (AM-26)*. Princeton University Press, 1950. ISBN 9780691083964. URL http://www.jstor.org/stable/j.ctt1b9rzn0.

SciPy. scipy.optimize.linear_sum_assignment, 2025. URL https://docs.scipy.org/doc/scipy/reference/generated/scipy.optimize.linear_sum_assignment.html. SciPy Documentation.

I. Serban, B. Béri, A. R. Akhmerov, and C. W. J. Beenakker. Domain wall in a chiral p-wave superconductor: A pathway for electrical current. *Phys. Rev. Lett.*, 104:147001, 4 2010. doi: 10.1103/PhysRevLett.104.147001. URL https://arxiv.org/abs/0912.3937.

Noam Shazeer. Fast transformer decoding: One write-head is all you need, 2019. URL https://arxiv.org/abs/1911.02150.

Noam Shazeer. Glu variants improve transformer, 2020. URL https://arxiv.org/abs/2002.05202.

I. H. Sloan and E. P. Stephan. Collocation with chebyshev polynomials for symm's integral equation on an interval. *Journal of the Australian Mathematical Society, Series B*, 34:199–211, 1992.

Jianlin Su, Yu Lu, Shengfeng Pan, Ahmed Murtadha, Bo Wen, and Yunfeng Liu. Roformer: Enhanced transformer with rotary position embedding, 2023. URL https://arxiv.org/abs/2104.09864.

Qwen Team. Qwen1.5-moe: Matching 7b model performance with 1/3 activated parameters. URL https://qwenlm.github.io/blog/qwen-moe/.

Hugo Touchette. The large deviation approach to statistical mechanics. *Physics Reports*, 478(1): 1–69, 2009. ISSN 0370-1573. doi: https://doi.org/10.1016/j.physrep.2009.05.002. URL https://arxiv.org/abs/0804.0327.

Ashish Vaswani, Noam Shazeer, Niki Parmar, Jakob Uszkoreit, Llion Jones, Aidan N. Gomez, Łukasz Kaiser, and Illia Polosukhin. Attention is all you need. In *Advances in Neural Information Processing Systems*, 2017. arXiv:1706.03762.

Hermann Weyl. *The Classical Groups: Their Invariants and Representations*. Princeton Landmarks in Mathematics and Physics. Princeton University Press, 2016. ISBN 9781400883905. URL https://books.google.com/books?id=2twDDAAAQBAJ.

Jiashu Xu, Fei Wang, Mingyu Ma, Pang Wei Koh, Chaowei Xiao, and Muhao Chen. Instructional fingerprinting of large language models. In Kevin Duh, Helena Gomez, and Steven Bethard (eds.), *Proceedings of the 2024 Conference of the North American Chapter of the Association for Computational Linguistics: Human Language Technologies (Volume 1: Long Papers)*, pp. 3277–3306, Mexico City, Mexico, June 2024. Association for Computational Linguistics. doi: 10.18653/v1/2024.naacl-long.180. URL https://aclanthology.org/2024.naacl-long.180/.

An Yang, Baosong Yang, Binyuan Hui, Bo Zheng, Bowen Yu, Chang Zhou, Chengpeng Li, Chengyuan Li, Dayiheng Liu, Fei Huang, Guanting Dong, Haoran Wei, Huan Lin, Jialong Tang, Jialin Wang, Jian Yang, Jianhong Tu, Jianwei Zhang, Jianxin Ma, Jianxin Yang, Jin Xu, Jingren Zhou, Jinze Bai, Jinzheng He, Junyang Lin, Kai Dang, Keming Lu, Keqin Chen, Kexin Yang, Mei Li, Mingfeng Xue, Na Ni, Pei Zhang, Peng Wang, Ru Peng, Rui Men, Ruize Gao, Runji Lin, Shijie Wang, Shuai Bai, Sinan Tan, Tianhang Zhu, Tianhao Li, Tianyu Liu, Wenbin Ge, Xiaodong Deng, Xiaohuan Zhou, Xingzhang Ren, Xinyu Zhang, Xipin Wei, Xuancheng Ren, Xuejing Liu, Yang Fan, Yang Yao, Yichang Zhang, Yu Wan, Yunfei Chu, Yuqiong Liu, Zeyu Cui, Zhenru Zhang, Zhifang Guo, and Zhihao Fan. Qwen2 technical report, 2024. URL https://arxiv.org/abs/2407.10671.

An Yang, Anfeng Li, Baosong Yang, Beichen Zhang, Binyuan Hui, Bo Zheng, Bowen Yu, Chang Gao, Chengen Huang, Chenxu Lv, Chujie Zheng, Dayiheng Liu, Fan Zhou, Fei Huang, Feng Hu, Hao Ge, Haoran Wei, Huan Lin, Jialong Tang, Jian Yang, Jianhong Tu, Jianwei Zhang, Jianxin Yang, Jiaxi Yang, Jing Zhou, Jingren Zhou, Junyang Lin, Kai Dang, Keqin Bao, Kexin Yang, Le Yu, Lianghao Deng, Mei Li, Mingfeng Xue, Mingze Li, Pei Zhang, Peng Wang, Qin Zhu, Rui Men, Ruize Gao, Shixuan Liu, Shuang Luo, Tianhao Li, Tianyi Tang, Wenbiao Yin, Xingzhang Ren, Xinyu Wang, Xinyu Zhang, Xuancheng Ren, Yang Fan, Yang Su, Yichang Zhang, Yinger Zhang, Yu Wan, Yuqiong Liu, Zekun Wang, Zeyu Cui, Zhenru Zhang, Zhipeng Zhou, and Zihan Qiu. Qwen3 technical report, 2025. URL https://arxiv.org/abs/2505.09388.

Yiqun Yao, Zheng Zhang, Jing Li, and Yequan Wang. Masked structural growth for 2x faster language model pre-training. In *The Twelfth International Conference on Learning Representations*, 2024. URL https://openreview.net/forum?id=rL7xsg1aRn.

Boyi Zeng, Chenghu Zhou, Xinbing Wang, and Zhouhan Lin. Huref: HUman-REadable fingerprint for large language models, 2024. URL https://openreview.net/forum?id=ibggY9ZJ1T.

Biao Zhang and Rico Sennrich. Root mean square layer normalization, 2019. URL https://arxiv.org/abs/1910.07467.

Jie Zhang, Dongrui Liu, Chen Qian, Linfeng Zhang, Yong Liu, Yu Qiao, and Jing Shao. REEF: Representation encoding fingerprints for large language models. In *The Thirteenth International Conference on Learning Representations*, 2025. URL https://openreview.net/forum?id=SnDmPkOJ0T.

Fan Zhou, Zengzhi Wang, Qian Liu, Junlong Li, and Pengfei Liu. Programming every example: Lifting pre-training data quality like experts at scale, 2025. URL https://arxiv.org/abs/2409.17115.

A Mathematical Background

Our work primarily builds upon the foundation of matrix analysis. To avoid excessive technicality or verbosity, we only introduce the key tools and properties used in this paper, potentially omitting or abbreviating proofs. Interested readers are encouraged to refer to Horn & Johnson (2012) for a comprehensive overview of matrix analysis.

A.1 Matrix Analysis: Singular Value and Polar Decompositions

Singular Value Decomposition. The singular value decomposition (SVD) of a matrix $A \in \mathbb{R}^{m\times n}$ is given by

$$A = USV^{\mathrm{T}},$$

where $U \in \mathbb{R}^{m\times m}$ and $V \in \mathbb{R}^{n\times n}$ are orthogonal matrices, and $S \in \mathbb{R}^{m\times n}$ is a diagonal matrix with non-negative singular values on the diagonal:

$$\sigma_1 \geq \sigma_2 \geq \cdots \geq \sigma_r > 0 \quad (r = \mathrm{rank}(A)).$$

We denote $\sigma_i(A)$ as the i-th singular value of A.

Polar Decomposition. The polar decomposition of A has two common but distinct forms: the left decomposition $A = PW$ and the right decomposition $A = WQ$, where $P = (AA^{\mathrm{T}})^{1/2}$ and $Q = (A^{\mathrm{T}}A)^{1/2}$ are symmetric positive semidefinite matrices, and $W \in \mathbb{R}^{m\times n}$ (with orthonormal columns) is shared between both decompositions. We define the *orthogonal part* of A as $\mathrm{Ortho}(A) := W$. When A is full-rank, the orthogonal part of A is unique.

Connection to SVD. The orthogonal part W in the polar decomposition can be obtained from the SVD:

$$W = UV^{\mathrm{T}},$$

where U and V are derived from the SVD of A. The symmetric factors satisfy $P = USU^{\mathrm{T}}$ and $Q = VSV^{\mathrm{T}}$. However, when A is not invertible (with many singular values either exactly zero or close to zero), the computation of $W = UV^{\mathrm{T}}$ becomes ill-conditioned.

SVD and Spectral Calculus. Assume $A \in \mathbb{R}^{m\times n}$ has SVD $A = USV^{\mathrm{T}}$. Then:

$$AA^{\mathrm{T}} = U(SS^{\mathrm{T}})U^{\mathrm{T}}, \quad A^{\mathrm{T}}A = V(S^{\mathrm{T}}S)V^{\mathrm{T}}.$$

For any polynomial function $f \in \mathbb{R}[x]$ and $g(x) = xf(x^2)$, we have:

$$\begin{aligned} &f(AA^{\mathrm{T}})A \\ &= Uf(SS^{\mathrm{T}})U^{\mathrm{T}}USV^{\mathrm{T}} = Uf(SS^{\mathrm{T}})SV^{\mathrm{T}} \\ &= Ug(S)V^{\mathrm{T}} \\ &= USf(S^{\mathrm{T}}S)V^{\mathrm{T}} = USV^{\mathrm{T}}Vf(S^{\mathrm{T}}S)V^{\mathrm{T}} \\ &= Af(A^{\mathrm{T}}A). \end{aligned}$$

In fact, $g(S)$ can represent any odd polynomial. For any odd function G, we may find a polynomial f such that $f(x)$ agrees with $G(x)/x$ on all nonzero diagonal entries of SS^{T}. In particular, setting $G(x) = \mathrm{sign}(x)$, this spectral calculus yields the most "sensible" orthogonal part of A. We adopt the methods from Amsel et al. (2025) for a fast and relatively accurate implementation.

Trace Maximization Property. The orthogonal part W solves the optimization problem:

$$\max_{\{X \mid X^{\mathrm{T}}X = I\}} \left(\mathrm{Tr}(AX^{\mathrm{T}})\right).$$

The maximum value is the sum of all the singular values of A, i.e., $\mathrm{Tr}(P) = \sum_{i=1}^{r} \sigma_i$.

Orthogonal Invariance of Singular Values. The singular values $\{\sigma_i\}$ of A are invariant under both left and right orthogonal transformations:

$$\sigma_i(UAV) = \sigma_i(A), \quad \forall U, V \text{ orthogonal and } i = 1, \cdots, \min(m, n).$$

Thus, any function depending on these singular values remains invariant under orthogonal transformations. Examples include:

- **Frobenius Norm**: $\|A\|_F = \sqrt{\sum_i \sigma_i^2(A)}$;
- **Spectral Norm**: $\|A\|_S = \sigma_1(A)$;
- **Ky Fan k-Norm**: $\|A\|_{KF} = \sum_{i=1}^{k} \sigma_i(A)$;
- **Schatten p-Norm** (Schatten, 1950): $\|A\|_p = \sqrt[p]{\sum_i \sigma_i^p(A)}$.

Any combination of these functions also remains invariant under orthogonal transformations. These functions may serve as preliminary indicators for detecting model similarity.

Orthogonal Matrices and RMSNorms Commute. For any orthogonal matrix U, we have:

$$\mathrm{RMSNorm}(x)U = \mathrm{RMSNorm}(xU),$$

for any nonzero vector $x \in \mathbb{R}^n$ (row vector). Moreover, all transformations satisfying this property $(\mathrm{RMSNorm}(\cdot))U = \mathrm{RMSNorm}((\cdot)U)$ are orthogonal transformations.

To prove this, note that $\mathrm{RMSNorm}(y)$ is always a constant multiple ($\sqrt{n}$) of a unit vector when $y \neq 0$. Thus, U maps all unit vectors to unit vectors. By linearity, this implies $\|xU\| = \|x\|$ and $xUU^{\mathrm{T}}x^{\mathrm{T}} = xx^{\mathrm{T}}$. Taking x over all eigenspaces of UU^{T}, we see that 1 is the only eigenvalue of UU^{T}. Hence, $UU^{\mathrm{T}} = \mathbf{1}_n$, and U is orthogonal.

A.2 Large Deviation Theory

Our research extensively involves random orthogonal matrices, particularly focusing on traces of such matrices. To obtain statistically meaningful p-values, traditional statistical p-tests become useless for our case, due to the interdependence of the elements within an orthogonal matrix. Instead, we rely on large deviation theory for deriving the p-value. For a comprehensive exposition of this theory, please refer to Dembo & Zeitouni (1998) and Anderson et al. (2010).

B Solving All Transformations

If the significance of the p-value has already been determined from the p-values for vocabulary embeddings, this step is entirely optional. However, if the no significant p-value is observed at this stage, we cannot yet rule out the possibility of model homology. This may occur when an adversary used a general orthogonal matrix for obfuscation. Additionally, interested readers may wish to determine the exact relationship between two models, potentially with different architectures.

Since $P = \arg\max \mathrm{Tr}(P\tilde{U}^{\mathrm{T}})$, we proceed as follows: If P is reliably identified as a permutation matrix ($p < 2 \times 10^{-23}$), set $U := P$; otherwise, set $U := \tilde{U}$.

Solving the Relationship between Layers. In practical scenarios, the number of layers for two models are not necessarily the same. It is important to first determine the relationship between the layers of both models via solving a maximal ordered matching problem. We select a representative matrix (for example, attention K or V) for each layer i of model A and layer j of model B. For each pair (i, j) we do the process below and obtain a similarity measure matrix of shape $L \times L'$. Solving the maximal ordered matching for this matrix will give the relationship between all layers. See Section E.1 for a specefic example how this works.

Solving the Transformations in the Attention Module. We now solve for the inner transformations W_Q, W_K, W_V, and W_O based on the heuristic U.

Our objectives are:

$$\min_{W_Q \text{ orthogonal}} \|UQW_Q - Q'\|_F^2, \quad \min_{W_K \text{ orthogonal}} \|UKW_K - K'\|_F^2,$$

for Q and K. By the trace maximization property, the solutions for W_Q and W_K are given by:

$$W_Q = \lambda \mathrm{Ortho}(Q^{\mathrm{T}}U^{\mathrm{T}}Q'), \quad W_K = \mu \mathrm{Ortho}(K^{\mathrm{T}}U^{\mathrm{T}}K'),$$

where the similarity measure can be calculated as

$$t_\square = \texttt{linear\_sum\_assignment}(W_\square), \quad \square \in Q, K.$$

Also, scaling coefficients λ and μ are computed as:

$$\lambda = \frac{\|Q'\|_F}{\|Q\|_F}, \quad \mu = \frac{\|K'\|_F}{\|K\|_F}.$$

For W_V and W_O, we may apply the same method to compute $\mathrm{Ortho}(V^{\mathrm{T}}U^{\mathrm{T}}V')$ and $\mathrm{Ortho}(OU^{\mathrm{T}}O'^{\mathrm{T}})$. However, since W_V and W_O may involve general invertible transformations, our method does not guarantee recovering the exact transformation. solving the general case without additional assumptions is challenging. We leave this problem for future work.

Solving the MLP. At this point, there is only one matrix left to solve: the permutation of intermediate neurons, denoted by P. The solution is given as follows:

$$U_X = \mathrm{Ortho}(X^{\mathrm{T}}U^{\mathrm{T}}X'), \quad X \in \{\mathrm{Gate}, \mathrm{Up}, \mathrm{Down}\};$$
$$P = \arg \max_{P \in \mathrm{Perm}(\mathrm{IntermediateDim})} \mathrm{Tr}\left(P\left(U_{\mathrm{Gate}} + U_{\mathrm{Up}} + U_{\mathrm{Down}}\right)^{\mathrm{T}}\right).$$

Typically, we expect the three solutions $\arg\max \mathrm{Tr}\left(PU_X^{\mathrm{T}}\right)$, for $X \in \{\mathrm{Gate}, \mathrm{Up}, \mathrm{Down}\}$, to yield the same permutation. However, computing the orthonormal part for intermediate matrices (which often have 14,000–20,000 rows) is computationally expensive. Adding the three terms together would triple the computation cost. If the noise level is tolerable, we may simply select one of them:

$$P = \arg \max_{P \in \mathrm{Perm}(\mathrm{IntermediateDim})} \mathrm{Tr}\left(PU_{\mathrm{Up}}^{\mathrm{T}}\right).$$

C Overall Algorithm

We summarize our algorithm as follows:

Algorithm 1 Computing the p-value: $\mathrm{PValue}(P, U, d)$

Input: Permutation matrix P, orthogonal matrix U, dimension d
Compute $p := d! \cdot \exp(-(\mathrm{Tr}(PU^{\mathrm{T}}))^2/2)$ via $\log(p) \approx (d\log d - d) - (\mathrm{Tr}(PU^{\mathrm{T}}))^2/2$
Output: p

D Estimation of p-value via Large Deviation Theory

Let $\tilde{U}$ be a random orthogonal matrix, distributed uniformly according to the normalized Haar measure. We aim to estimate the following function, especially its long-tail behavior, for $c > 0$:

$$f(c) = \mathbb{P}\left[\mathrm{Tr}(\tilde{U}) \geq c\right].$$

The distribution of $f(c)$ is a well-studied problem in random matrix theory. Diaconis & Shahshahani (1994) proved that $\mathrm{Tr}(\tilde{U}) \to \mathcal{N}(0,1)$ in distribution. Later, Johansson (1997) showed that the convergence of $\mathrm{Tr}(\tilde{U})$ to $\mathcal{N}(0,1)$ is exponential under the total variation distance:

$$\mathrm{TV}(f - (1-\Phi)) \leq \exp(-\alpha n), \quad \text{for some } \alpha > 0,$$

where $\Phi(x)$ is the cumulative distribution function of the standard normal distribution.

It is known that $(1-\Phi)(x)$ has the following asymptotic behavior for large x:

$$(1-\Phi)(x) \approx \frac{1}{\sqrt{2\pi}x} \exp\left(-\frac{x^2}{2}\right), \quad (x \gg 1).$$

However, when both n and x are large, $\exp(-\alpha n)$ remains significantly larger than $\frac{1}{\sqrt{2\pi}x} \exp\left(-\frac{x^2}{2}\right)$. Thus, it is inappropriate to use $(1-\Phi)$ as the asymptotics of $f(c)$.

To study the tail behavior of $f(c)$, we leverage tools from Large Deviation Theory. Since n is typically large and the embedding dimension n is usually an even number in most models, we

Algorithm 2 MDIR (Matrix-Driven Instant Review)

Input: Model A, Model B
Initialize: Threshold $p_0 =$ some threshold (e.g. $\Phi(-10)$), relation flag $r = \mathsf{False}$
$L :=$ Number of layers in the model
$E :=$ Embedding matrix of A
$E' :=$ Embedding matrix of B
$\mathcal{C} :=$ Set of common vocabulary tokens between A and B
Compute $\tilde{U} := \mathrm{Ortho}(E[\mathcal{C},:]^{\mathsf{T}} E'[\mathcal{C},:])$ via polar decomposition
$P := \arg\max_{P \in \mathrm{Perm}(\mathrm{EmbDim})} \mathrm{Tr}(P\tilde{U}^{\mathsf{T}})$
Compute $p := \mathrm{PValue}(P, \tilde{U}, \mathrm{EmbDim})$
if $p < p_0$ **then**
  Set $r := \mathsf{True}$
  Set $U := P$
else
  Set $U := \tilde{U}$
end if
Yield: Transformation matrix U, p-value p
for Layer $i \in [L]$ **do**
  Extract attention weights Q, K, V, O from layer i of A
  Extract attention weights Q', K', V', O' from layer i of B
  for $X \in \{Q, K, V\}$ **do**
    Compute $W_X := \mathrm{Ortho}(X^{\mathsf{T}} U^{\mathsf{T}} X') \cdot \frac{\|X'\|_F}{\|X\|_F}$
  end for
  Extract MLP weights $\mathrm{Gate}, \mathrm{Up}, \mathrm{Down}$ from layer i of A
  Extract MLP weights $\mathrm{Gate}', \mathrm{Up}', \mathrm{Down}'$ from layer i of B
  Compute $U_X := \mathrm{Ortho}(X^{\mathsf{T}} U^{\mathsf{T}} X')$ for $X \in \{\mathrm{Up}\}$ (or $X \in \{\mathrm{Gate}, \mathrm{Up}, \mathrm{Down}\}$)
  $P := \arg\max_{P \in \mathrm{Perm}(\mathrm{IntermediateDim})} \mathrm{Tr}(P U_{\mathrm{Up}}^{\mathsf{T}})$
end for
Output: Relation flag r

assume $n = 2m$ without loss of generality. Additionally, we assume $\det(\tilde{U}) = 1$, or equivalently $\tilde{U} \in \mathrm{SO}(2m)$, since this introduces only an infinitesimal difference in the thermodynamic limit ($n \to \infty$). These assumptions simplify our analysis while preserving accuracy.

Theorem 1. *Let $A \in \mathrm{SO}(2m)$ be uniformly distributed according to the normalized Haar probability measure, and let $0 < r \leq 1/2$. The probability*

$$P(r, m) = \mathbb{P}\left[\frac{1}{2m}\operatorname{Tr}(A) \geq r\right]$$

satisfies the following large deviation principle:

$$\lim_{m\to\infty} \frac{-\log P(r, m)}{2m^2 r^2} = 1,$$

or equivalently,

$$P(r, m) \asymp \exp(-m^2 I(r)),$$

where

$$I(r) = 2r^2$$

is the good rate function.

For $r > 1/2$, a faster decay rate can be achieved: $I(r) > 2r^2$.

Before we delve into the proof, it is worth discussing the challenges we encountered. We are dealing with the Circular Real Ensemble (CRE, named after Serban et al. (2010)), which has a formulation distinct from traditional circular ensembles, such as Circular Unitary Ensembles (CUE) or Circular Orthogonal Ensembles (COE) (Dyson, 1962). These ensembles play important roles in both random matrix theory and condensed matter physics.

One of the problems most similar to ours is the Gross-Witten Ensemble (Gross & Witten, 1980; Gamboa et al., 2017), which concerns the large deviations from the typical value of $\operatorname{Re}\operatorname{Tr}(U)$ as $N \to \infty$ (where $U \in \mathrm{U}(N)$ is a random unitary matrix). Our problem can be regarded as a real orthogonal variant of Gross-Witten Ensemble, but this is undocumented in previous literature.

Unitary matrices possess many elegant properties. One of them is the Cayley transformation, defined as $\phi(z) := \mathrm{i}(1 + z)/(1 - z)$, which maps the punctured unit circle $\mathbb{T} \setminus \{1\}$ to the real line $\mathbb{R}$. When the Cayley transformation is applied to a unitary matrix, it sends unit eigenvalues to the real line, thereby producing a Hermitian matrix (i.e., $\phi(U)$ is Hermitian for $U \in \mathrm{U}(N)$). However, under the Cayley transformation, an orthogonal matrix is transformed into a purely imaginary, anti-symmetric matrix, which is of little interest. In the field of deep learning, complex values rarely appear, and we shall focus on the Circular Real Ensemble in our proof.

The circular ensemble is closely related to thermodynamics and large deviation theory. We refer to Mehta's book *Random Matrices* (Mehta, 2004), and a comprehensive introduction can be found in Chapter 12 of it.

D.1 Proof of Theorem 1

Proof. If A is uniformly distributed according to the Haar measure in $\mathrm{SO}(2m)$ (a manifold of real dimension $m(2m - 1)$), all eigenvalues of A lie on the unit circle, and complex eigenvalues form paired conjugates, possibly accompanied by several $+1$ and -1.

When $\det A = 1$, the product of complex eigenvalues yields $+1$, and there are almost surely no -1 or $+1$ eigenvalues.

Denote by $\{e^{i\theta_k}, e^{-i\theta_k} : k = 1, 2, \cdots, m\}$ the eigenvalues of A. It is a classical result (see Weyl (2016); Girko (1985)) that the phases $(\theta_k)_k$ obey the distribution characterized by the following probability density:

$$p(\theta_1, \cdots, \theta_m)\mathrm{d}\theta_1 \cdots \mathrm{d}\theta_m = C \prod_{1\leq k<j\leq m} (\cos\theta_k - \cos\theta_j)^2 \mathrm{d}\theta_1 \cdots \mathrm{d}\theta_m,$$

and the trace $\operatorname{Tr}(A)$ is the sum of all eigenvalues:

$$\operatorname{Tr}(A) = 2\sum_{i=1}^{m} \cos(\theta_i).$$

By substitution of variables, let $t_i = \cos(\theta_i) \in [-1, 1]$, and $\mathrm{d}t_i/\sqrt{1-t_i^2} = \mathrm{d}\theta_i$. We study the substituted distribution:

$$p(t_1, \cdots, t_m)\mathrm{d}t_1 \cdots \mathrm{d}t_m = C' \prod_{1 \le k < j \le m} (t_k - t_j)^2 \cdot \prod_{1 \le i \le m} (1 - t_i^2)^{-1/2} \mathrm{d}t_1 \cdots \mathrm{d}t_m.$$

Taking the logarithm, we have

$$-\log p(t_1, \cdots, t_m) = \sum_{1 \le k < j \le m} (-2 \log |t_k - t_j|) + \sum_{1 \le i \le m} \left(\frac{\log(1 - t_i^2)}{2} \right) + C_0.$$

This has a clear thermodynamical interpretation: Consider m interacting particles located on the interval $[-1, 1]$, with coordinates $t_1, \cdots, t_m$. The energy $E(t_1, \cdots, t_m)$ is the sum of the following two kinds of potentials:

1. Repelling force: for particles k and j, their interaction potential is $-2 \log |t_k - t_j|$, meaning that they repel each other according to the 2-dimensional Coulomb law;
2. External field: particles are attracted to the boundary points -1 and $+1$, with the potential $\sum_{1 \le i \le m} \left(\frac{\log(1-t_i^2)}{2} \right)$.

Inspired by Chapter 12 of Mehta (2004) and also Touchette (2009), we define the Canonical Ensemble of these m particles as follows, which admits a partition function:

$$Z(t_1, \cdots, t_m) = \int_{-1}^{1} \cdots \int_{-1}^{1} \exp(-\beta E(t_1, \cdots, t_m)) \mathrm{d}t_1 \cdots \mathrm{d}t_m,$$

where

$$\begin{aligned} E(t_1, \cdots, t_m) &= \sum_{1 \le k < j \le m} (-2 \log |t_k - t_j|) + \sum_{1 \le i \le m} \left(\frac{\log(1 - t_i^2)}{2} \right) \\ &= -\log p(t_1, \cdots, t_m) - C_0. \end{aligned}$$

We set the thermodynamic beta to be $\beta = 1/(k_B T) = 1$ because we do not study temperature changes.

We are interested in the probability:

$$P(r, m) = \mathbb{P}\left[\frac{1}{2m} \operatorname{Tr}(A) \ge r \right].$$

Using the representation $\operatorname{Tr}(A) = 2 \sum_{k=1}^{m} \cos(\theta_k) = 2 \sum_{k=1}^{m} t_k$, this becomes:

$$P(r, m) = \mathbb{P}\left[\frac{1}{m} \sum_{k=1}^{m} t_k \ge r \right].$$

Let

$$\mu_m = \frac{1}{m} \sum_{k=1}^{m} \delta_{t_k}$$

be the empirical measure of the eigenvalue distribution. In the thermodynamic limit $m \to \infty$, μ_m should converge weakly to an equilibrium measure μ that minimizes the free energy functional $F(\mu)$.

We now solve the exact form of $F(\mu)$. We refer to Theorem 2.1 of the paper (Eichelsbacher et al., 2011), where we are dealing with the case $\theta = 1$, $\kappa = 1$, and $w_m(x) = (1 - x^2)^{1/(2m)}$, where $w_m(x) \to 1$ in the thermodynamic limit $m \to \infty$. This suggests that the interaction term dominates, and the external field term is negligible when m is large.

The form of $F(\mu)$ is therefore given by

$$F(\mu) = \iint_{[-1,1]^2} \left(\log \frac{1}{|x - y|} \right) \mathrm{d}\mu(x) \mathrm{d}\mu(y),$$

with the rate function

$$\tilde{I}(\mu) = \iint_{[-1,1]^2} \left(\log \frac{1}{|x-y|} \right) \mathrm{d}\mu(x)\mathrm{d}\mu(y) - c,$$

where $c = \inf_\mu F(\mu)$. Note that the rate function $\tilde{I}(\mu)$ is defined for the probability measure μ, not yet ready for our $I(r)$.

From Corollary 2.2 of the paper (Eichelsbacher et al., 2011), it suffices to solve the following two variational problems:

$$\inf_{\mu} F(\mu); \qquad \inf_{\mu:\, \int x \mathrm{d}\mu \geq r} F(\mu).$$

To solve these two problems, we parametrize μ using Chebyshev polynomials, with the additional assumption that μ is absolutely continuous with respect to the Lebesgue measure $\mathrm{d}x$ and normalized Chebyshev measure $\mathrm{d}x/(\pi\sqrt{1-x^2})$.

We suppose that μ is parametrized by the following series:

$$\mu(x) = \frac{1}{\pi\sqrt{1-x^2}} \sum_{i=0}^{\infty} a_i T_i(x),$$

where T_i is the i-th Chebyshev polynomial of the first kind, and $F(\mu)$ now becomes a quadratic form of these coefficients $\{a_i\}$. An additional constraint must not be overlooked: μ is a probability measure, and

$$\int_{-1}^{1} \mathrm{d}\mu = \frac{T_0(x)}{\pi\sqrt{1-x^2}} \sum_{i=0}^{\infty} a_i T_i(x) \mathrm{d}x = a_0 = 1.$$

It is known that $\log|x-y|$ has the Chebyshev expansion (Sloan & Stephan, 1992; Mason & Handscomb, 2002):

$$\log|x-y| = -\log 2 - \sum_{n=1}^{\infty} \frac{2}{n} T_n(x) T_n(y),$$

so

$$\begin{aligned} F(\mu) = &\iint_{[-1,1]^2} \left(\log 2 + \sum_{n=1}^{\infty} \frac{2}{n} T_n(x) T_n(y) \right) \frac{1}{\pi^2 \sqrt{1-x^2}\sqrt{1-y^2}} \\ &\left(\sum_{i=0}^{\infty} a_i T_i(x) \right) \left(\sum_{i=0}^{\infty} a_i T_i(y) \right) \mathrm{d}x\mathrm{d}y \\ = \log 2 \cdot &\iint_{[-1,1]^2} \frac{1}{\pi^2 \sqrt{1-x^2}\sqrt{1-y^2}} \mathrm{d}x\mathrm{d}y \\ + &\iint_{[-1,1]^2} \left(\sum_{n=1}^{\infty} \frac{2}{n} T_n(x) T_n(y) \right) \frac{1}{\pi^2 \sqrt{1-x^2}\sqrt{1-y^2}} \\ &\left(\sum_{i=1}^{\infty} a_i T_i(x) \right) \left(\sum_{i=1}^{\infty} a_i T_i(y) \right) \mathrm{d}x\mathrm{d}y. \end{aligned}$$

We recall the orthogonal relation of Chebyshev polynomials,

$$\int_{-1}^{1} \frac{T_a(x) T_b(x)}{\pi\sqrt{1-x^2}} \mathrm{d}x = \begin{cases} 1, & a = b = 0; \\ \frac{1}{2}, & a = b \neq 0; \\ 0, & a \neq b. \end{cases}$$

Using the orthogonal relation, we further simplify $F(\mu)$ as

$$F(\mu) = \log 2 + \sum_{i=1}^{\infty} \frac{a_i^2}{2i}.$$

Therefore, the problem $\inf_\mu F(\mu)$ admits a simple solution: $a_i = 0$ for every $i \geq 1$, and

$$\begin{aligned} \mathrm{d}\mu_0 &= \frac{\mathrm{d}x}{\pi\sqrt{1-x^2}}; \\ F(\mu_0) &= \log 2. \end{aligned}$$

Now we solve the equilibrium measure under one additional constraint $\int x\mathrm{d}\mu \geq r$:

$$\inf_{\mu:\ \int x\mathrm{d}\mu \geq r} F(\mu).$$

Since

$$\int_{-1}^{1} \mathrm{d}\mu = \frac{T_1(x)}{\pi\sqrt{1-x^2}} \sum_{i=0}^{\infty} a_i T_i(x)\mathrm{d}x = \frac{a_1}{2} = r,$$

this suggests that the equilibrium measure μ_r is

$$\mu_r(x) = \frac{1+2rx}{\pi\sqrt{1-x^2}} \quad (r \leq 1/2),$$

and

$$\inf_{\mu:\ \int x\mathrm{d}\mu \geq r} F(\mu) = F(\mu_r) = \log 2 + 2r^2.$$

Now we are close to completion: our rate function $\tilde{I}(\mu)$ is computed as

$$\tilde{I}(\mu) = F(\mu) - c = F(\mu) - F(\mu_0) = F(\mu) - \log 2.$$

We conclude that the rate is

$$\begin{aligned} &\exp\left(-m^2 \cdot \inf_{\mu:\ \int x\mathrm{d}\mu \geq r} \tilde{I}(\mu)\right) \\ &= \exp\left(-m^2 \cdot (\inf_{\mu:\ \int x\mathrm{d}\mu \geq r} \tilde{F}(\mu) - F(\mu_0))\right) \\ &= \exp\left(-m^2 \cdot 2r^2\right), \end{aligned}$$

which shows a good rate function for r: $I(r) = 2r^2$.

The function μ_r induces a measure if and only if $r \leq 1/2$. When $r > 1/2$, the function μ_r no longer induces a measure, as it violates positivity near $x = -1$. This suggests that our theoretical bound, $\log 2 + (2r)^2$, cannot be attained here (To satisfy the positivity of μ, the coefficients $a_2, a_3, \cdots$ cannot all be zero simultaneously).

Overall, we have

$$\inf_{\mu:\ \int x\mathrm{d}\mu \geq r} \tilde{I}(\mu) \geq (2r)^2$$

and

$$\begin{cases} I(r) = 2r^2, & \text{for } r \leq \dfrac{1}{2}; \\ I(r) > 2r^2, & \text{for } r > \dfrac{1}{2}. \end{cases}$$

□

D.2 Additional Notes on the $\mathrm{O}(2m) \setminus \mathrm{SO}(2m)$ Case

When $A \in \mathrm{O}(2m) \setminus \mathrm{SO}(2m)$, $\det(A) = -1$. There are two eigenvalues fixed at $+1$ and -1, respectively.

Our formula becomes:

$$p(t_1, \cdots, t_{m-1})\mathrm{d}t_1 \cdots \mathrm{d}t_{m-1} = C' \prod_{1 \leq k < j \leq m-1} (t_k - t_j)^2 \cdot \prod_{1 \leq i \leq m-1} (1-t_i^2)^{+1/2} \mathrm{d}t_1 \cdots \mathrm{d}t_{m-1}.$$

Taking the logarithm, we have

$$-\log p(t_1, \cdots, t_{m-1}) = \sum_{1 \le k < j \le m-1} (-2 \log |t_k - t_j|) - \sum_{1 \le i \le m-1} \left(\frac{\log(1 - t_i^2)}{2} \right) + C_0.$$

The only differences from above are that m is replaced by $m - 1$ and the external field term is negated. Both changes are negligible in the thermodynamic limit $m \to \infty$. Thus, we obtain the same conclusion for the rate function.

D.3 The Exact Form of Rate Function $I(r)$

We conjecture that the exact form of $I(r)$ is:

$$\begin{cases} I(r) = 2r^2, & \text{for } r \in \left(0, \frac{1}{2}\right]; \\ I(r) = \frac{1}{2} - \log 2 - \log(1 - r), & \text{for } r \in \left[\frac{1}{2}, 1\right). \end{cases}$$

Like the Gross-Witten Ensemble (Gross & Witten, 1980), there is a third-order phase transition near $r = 1/2$.

E Additional Experiments

E.1 Comparison with REEF

We benchmark our method against REEF (Representation Encoding Fingerprint) (Zhang et al., 2025) on two model pairs:

- **Llama-3.1-8B vs. Llama-3.2-1B** (Meta-AI, 2024): A pruned version where we expect a structured layer correspondence;
- **Llama-3.1-8B vs. Qwen3-8B-Base** (Yang et al., 2025): Two independently developed models with no known lineage.

Our results demonstrate that MDIR is capable of interpretably reconstructing layer mappings between related model weights. In Figure 8(a), MDIR produces a diagonal-like pattern, indicating that each layer of Llama-3.2-1B aligns with a specific layer in Llama-3.1-8B (the 16 layers of Llama-3.2-1B are derived from layer 0, 1, 2, 3, 4, 5, 8, 11, 14, 17, 20, 23, 26, 29, 30 and 31 of Llama-3.1-8B, respectively). This reveals not only homology but also the exact strategy used during model pruning. This offers MDIR a very fine-grained level of interpretability which previous methods cannot provide.

In contrast, REEF (Figure 8(c)) yields uniformly high CKA similarity measures across many pairs of layers and failing to identify the exact correspondence. While it captures global similarity, it lacks the granularity to reveal which layers are actually aligned, thus less effective for model homology detection.

When applied to unrelated models (Figure 8(b,d)), MDIR correctly outputs a noise pattern, consistent with the absence of structural homology. REEF, however, continues to report high similarities (> 0.9) between certain layer pairs.

E.2 Analysis of a Special Case

We present a case study of Qwen2.5-14B (Qwen et al., 2025) and Pangu-pro-MOE (Ascend Tribe, 2025; Ascend Team, 2025) in Figure 9.

F Generative AI Usage

We used generative AI tools, including large language models such as ChatGPT and Qwen, to assist with language editing and generate the code for figures visualizing experimental results. Specifically,

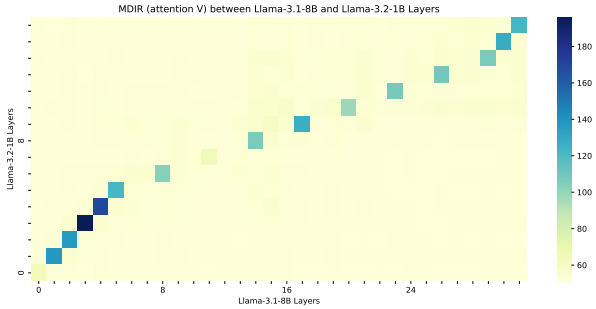

(a) MDIR, Llama-3.1-8B vs. Llama-3.2-1B

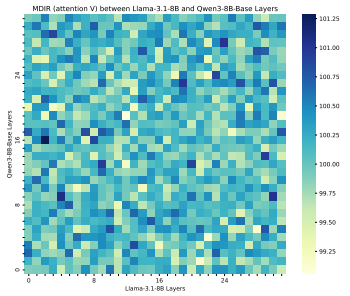

(b) MDIR, Llama-3.1-8B vs. Qwen3-8B-Base

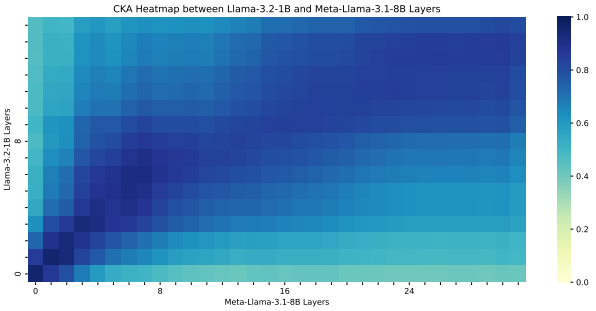

(c) REEF, Llama-3.1-8B vs. Llama-3.2-1B

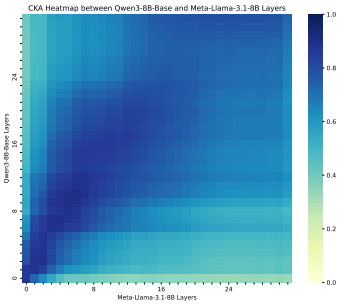

(d) REEF, Llama-3.1-8B vs. Qwen3-8B-Base

Figure 8: MDIR vs. REEF on some test cases.

ChatGPT and Qwen-VL were used to improve the clarity and fluency of the manuscript's writing (including translation of some sections from the original manuscript written in a different language), and to write code to produce plots based on the original data. All scientific content, including the methodology, experimental design and mathematical proof, was written originally and validated by the human authors. The use of generative AI was limited to drafting assistance and visualization support, and no AI system contributed to the core intellectual ideas or conclusions of this work. The authors take full responsibility for the accuracy and integrity of all content presented in this paper.

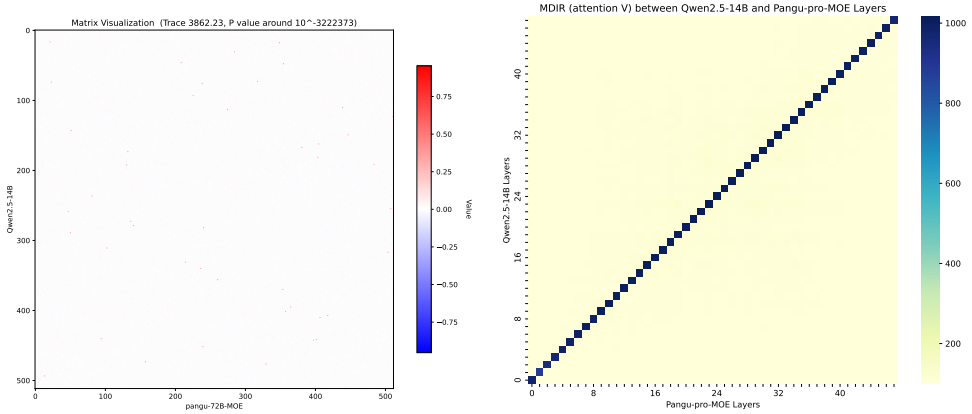

(a) Embedding (b) Layer Relations

(c) Layer 33 Attention V (d) Layer 19 MLP Up

Figure 9: A case study of Qwen2.5-14B and Pangu-pro-MOE. For large matrices, we plot the first 512×512 submatrix.